In Proceedings of the IEEE AUV Conference, Monterey, CA, USA, 2010.

Horizontal Mapping Accuracy in Hydrographic AUV Surveys

Øyvind Hegrenæs*, Torstein Olsmo Sæbø†, Per Espen Hagen*, Bjørn Jalving*

*Kongsberg Maritime Subsea, AUV Department, NO-3191 Horten, Norway
†Norwegian Defence Research Establishment, NO-2027 Kjeller, Norway

***Abstract*— Underwater vehicles are used in a wide range of tasks in various sectors. Cost-effective and accurate seabed surveying and mapping using autonomous underwater vehicles (AUVs) have been carried out for years in the offshore oil and gas sector. Much of the experience gained is now being benefited upon in new and challenging applications. One of the emerging AUV applications is hydrographic surveying (e.g. for creating nautical charts), particularly in waters shallower than 100 m. Key factors for mission-success include obtainable accuracy and resolution of the final digital terrain model (DTM), as well as the feature detection capability of the integrated system.**

This paper gives an in-depth discussion and analysis of the horizontal mapping accuracy achievable by integrated, state-of-the-art hydrographic AUV systems. The HUGIN 1000 AUV fitted with interferometric synthetic aperture sonar (SAS) is used as a case study, and the system accuracy as assessed in detail – starting from surface navigation, going all the way down to the acoustic seabed footprint. A discussion is given at the end on the feasibility of AUVs in terms of the minimum standards proposed by the International Hydrographic Organization (IHO).

I. Introduction

Autonomous underwater vehicles (AUVs) have proved impressive performance in commercial seabed mapping operations, both with respect to mapping efficiency and data quality. While traditional hydrographic surveys for creating e.g. nautical charts have been carried out using surface based systems, an increasing interest is shown toward the use of AUVs for the same purpose. Part of the reasons are probably the versatility and multi-disciplinary capability of the AUVs, the stability of the platform and the resulting high-quality high-resolution data, the crew size needed for operations, and not the least, the ability to carry out missions fully autonomously.

Knowing the accuracy or reliability of the final chart of digital terrain model (DTM) is imperative for the end-user or institution. As discussed in this paper, accuracy denotes the degree of conformity (offset) of a measured or estimated quantity to its true value. Similarly, precision is the degree to which repeated samples or measurements under unchanged conditions show the same results (variability). For some applications such as making nautical charts it is crucial that the accuracy is high. This is particularly the case in shallow water. Precision is on the other hand indicative of the ability to build fine resolution images, and may therefore be necessary for other applications, e.g. archeology or military operations using synthetic aperture sonar (SAS). The need for accuracy may vary in these cases. Due to their versatility, AUVs can facilitate a wide range of technical needs and applications.

For a DTM the quantities of interest are co-registered depth and position data. A key observation is that the survey end-product has no better accuracy than the least accurate component in the measurement chain, from surface navigation all the way down to the acoustic seabed footprint. The accuracy of each component or of the final DTM (total accuracy) may be stated by an uncertainty and some associate confidence level. The purpose of this paper is to discuss and analyze the achievable horizontal mapping accuracy in integrated, state-of-the-art hydrographic AUV systems. While the Kongsberg Maritime HUGIN 1000 AUV fitted with HISAS SAS is used as a case study, most of the results and methodologies apply to other AUVs and traditional hydrographic payloads such as multi-beam echo sounder (MBE) and side-scan sonar (SSS).

This paper is organized as follows. Section II gives a brief introduction to AUVs, including payload sensors and navigation. Some details on the HUGIN 1000 AUV and its sensors are given, including examples of data collected with the HISAS SAS. The paper continues in Section III with a breakdown and analyses of different error sources which contribute to the horizontal position uncertainty of the DTM soundings. Error budgets are presented in Section IV. A discussion is also given on the feasibility of AUVs in terms of the standards proposed by the International Hydrographic Organization (IHO). Conclusions are given in Section V.

II. AUVs for Hydrographic Surveying

A. Platforms and Payload Systems

AUVs are available as COTS (commercial, off-the-shelf) systems in a range of sizes and depth ratings. In general, endurance and capability scales with vehicle size. Smaller vehicles, such as the REMUS 100, can be equipped with small-footprint bathymetric sensors such as a GeoAcoustics GeoSwath. HUGIN 1000, the system described in this article, is a medium-size AUV capable of carrying and operating multiple high-end sensors simultaneously. The vehicle is shown in Fig. 1. The vehicle has a dry weight of 600-900 kg depending on configuration, a length of approximately 5 m, and a diameter of 75 cm. A typical military configuration includes the HISAS 1030 interferometric SAS, an EM 3002 MBE,

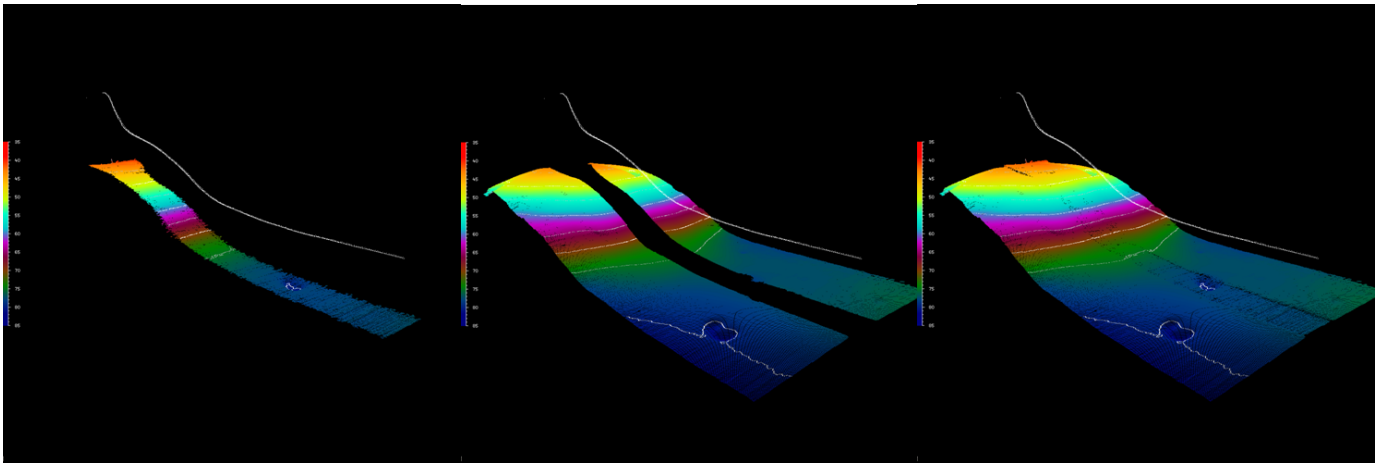

Fig. 2. Merged MBE and HISAS 1030 sidescan swath. The center figure shows the wide swath from the HISAS sidescan.

Fig. 1. A HUGIN 1000 AUV mounted on a Royal Norwegian Navy mine hunting vessel. The port side HISAS 1030 transducers are inside the transparent window in the center section.

an optical camera and LED strobe, and an imaging forward-looking sonar. Additional sensors such as CTD sensor and turbidity sensor may also be included. The interferometric SAS and the MBE can both produce high-quality, high-resolution bathymetry data suitable for hydrographic surveying. The depth rating of the HUGIN 1000 is 3000 m, with exception of the military version which is rated to 1000 m. The speed range is 1.5 to 6 knots, with a typical endurance of 18-30 h.

As mentioned AUVs have unique capabilities, also regarding bathymetric surveying. Bathymetric mapping was in fact the first application for the HUGIN vehicles; with the first commercial operation taking place in 1997 [1]. Especially in deep water, AUVs can provide bathymetric resolution unattainable from surface vessels, and with considerably higher speed and better data quality than what is offered by ROVs or towed systems. AUVs are normally operated at a nearly constant altitude above the seabed, providing constant swath-width regardless of the seafloor terrain.

SAS is most often thought of as an imaging sensor – an extremely high-quality SSS. Being a fully interferometric system however, HISAS also provides not one, but two bathymetry products: sidescan bathymetry, which is a low-cost single-ping based product, and SAS bathymetry. The sensing resolution is on the order of 1-2 m with sidescan bathymetry, and 10-20 cm with SAS bathymetry. Both products can be generated for the full swath. See [2] for more details.

It must also be noted that, by virtue of also being an imaging sensor, SAS imagery can be used to detect and classify features with size down to a few decimeters (or less, depending on geometry and echo strength). HISAS images have a constant resolution of better than 5x5 cm at all ranges. The availability of bathymetry also allows highly accurate positioning of any detected features (unlike a SSS or a non-interferometric SAS, where one normally has to assume a flat seafloor).

1) Coverage Rate: HISAS, like a SSS, covers a wide sector to each side of the vehicle, but has inadequate performance directly under the vehicle. A simple rule of thumb is that the maximum sonar range should be less than 10 times AUV altitude. Simultaneously, SAS range is limited by the fundamental requirement that the vehicle move less than half the length of the receiver array between pings. This results in a maximum range of approximately 200 m at 2 m/s speed. At water depths of 30-40 m or more, HISAS is typically operated at 20-25 m altitude and 3-4 knots speed. The actual coverage rate, compensating for the nadir gap and adding extra overlap to allow for navigation uncertainty, is greater than 2 km^2/h [3].

In shallower water, acoustic multipath can be an issue, and the system is most often operated at a constant depth of 2-5 m below the surface, to maximize coverage while avoiding transmission through the surface layers.

The area coverage rate can be increased further by using the MBE to cover the nadir gap, provided that (1) SAS

imaging is not required for the entire area, and (2) that the MBE bathymetry has sufficient resolution, accuracy and sample density. A good quality MBE like the EM 3002 has a resolution matching HISAS sidescan bathymetry, but not SAS bathymetry. An illustration showing the combined use of HISAS sidescan and MBE is shown in Fig. 2

One of the challenges of operating multiple sensors simultaneously is that requirements on operational parameters such as altitude and speed differ between sensors. Fortunately, for bathymetric mapping, there is a considerable range of settings where the SAS and the MBE both work very well. The MBE more than covers the nadir gap of the HISAS. The overlapping regions can be used for quality control, by comparing the data from the two sensors.

B. Navigation

The limitations of underwater sensors and the demand for autonomy makes underwater navigation a unique and difficult challenge. Most AUV navigation systems are today based on an inertial navigation system (INS), which takes measured angular rates and specific forces from an inertial measurement unit (IMU) as inputs. The INS then calculates the position, orientation and velocity of the vehicle relative to the inertial space. Due to inherent errors in the IMU however, a pure INS solution will drift of rapidly with time. A navigation grade INS such as the one installed in HUGIN 1000 drifts on the order of 0.8 nmi/h if left unaided. The aiding may be done using a wide range of sensors, including a depth sensor, acoustic positioning, GPS while at the surface, and some form of velocity aiding. Once a suitable aiding framework has been established, a Kalman filter (KF) is typically applied for carrying out the fusion of the disparate sensor data and the INS data. See [4], [5], [6] for a further discussion.

For hydrographic applications the use of ultra-short baseline (USBL) acoustic positioning is the preferred method. The use of Kongsberg Maritime HiPAP USBL is discussed later in this paper in regards to achievable mapping accuracy. The use of surface GPS fixes is also discussed. This may be the only feasible solution in very shallow water or when fully autonomous missions are desirable, or even required. The importance of proper velocity aiding in cases where positioning is sparse should be emphasized.

1) Accuracy Enhancement in Post-Processing: When discussing underwater navigation, it is important to distinguish between performance in real-time and after post-processing. The real-time performance obviously determines where the AUV actually collects its data. Depending on the application, it may be desirable to enhance the navigation precision further in post-processing. This is standard procedure for all the HUGIN AUVs, where the post-processing is carried out using NavLab [7]. NavLab is a simulation and navigation post-processing tool which has been used extensively with all the HUGIN AUVs since the late 1990's. In addition to re-navigating the real-time (based on experimental or simulated data) navigation system, NavLab also contains offline smoothing functionality, based on a Rauch-Tung-Striebel (RTS) implementation. The RTS smoother utilizes both past and future sensor measurements and KF covariances, hence significantly improving the integrity and accuracy of the final navigation solution [8].

III. Horizontal Mapping Accuracy

The total horizontal uncertainty (THU) of a DTM is to be understood as the uncertainty of the combined AUV positions and sounding footprint positions. As mentioned in Section II, there are in principle two ways of carrying out AUV missions; fully autonomous or supervised, and by utilizing AUV surface GPS or some form of acoustic positioning in order to bound the navigation system position error drift. Uncertainties related to these systems and other components further down in the measurement chain are discussed subsequently in relation to their contribution to the THU. Many of the contributions are included in the DTM error budget in Section IV. Part of the material is motivated by the work carried out in [9]. Some other relevant work can also be found in [10], [11], [12].

A. AUV Related Uncertainties

The following gives a discussion on uncertainties related to the horizontal positioning of the AUV. The HUGIN AUV and the HiPAP USBL system discussed in Section II are used as case studies. With few exceptions the material applies to other integrated hydrographic AUV systems as well.

1) GPS accuracy: Several GPS services applicable for AUV survey systems are available:

- GPS standard positioning service (SPS)
- GPS precise positioning service (PPS)
- Differential GPS (DGPS)
- Real-time kinematic GPS (RTKGPS)
- GPS precise point positioning (PPP)

SPS and PPS are both available worldwide, but PPS is only for authorized users and primarily intended for military purposes. Stand-alone single-frequency (L1) SPS solutions exist which have a horizontal accuracy on the order of 2 m (1σ). Dual frequency (L1/L2) yields slightly better performance. Further accuracy improvement is achieved by incorporating correction data broadcasted from stationary reference stations. This is the case for both DGPS and RTKGPS. The systems differ in the use of code-phase and carrier-phase techniques, where the latter yields the best performance. DGPS typically provides a horizontal accuracy on the order of 0.5 m (1σ) while RTKGPS has an accuracy ranging from about 0.2 m (1σ) down to a few centimeters or less. A post-processing alterative to DGPS and RTKGPS which does no rely on a reference station infrastructure is GPS PPP. By fusing raw carrier-phase data from a single GPS SPS receiver (typically dual-frequency) with precise ephemerides and satellite clock corrections (freely available from the Internet), PPP yields an accuracy close to RTKGPS. See [13], [14] for a further discussion on GPS PPP.

All the above mentioned GPS techniques and accuracy numbers are feasible for a surface ship, and hence for being used in the fusion with USBL acoustic position measurements. For the GPS mounted on an AUV the situation is more

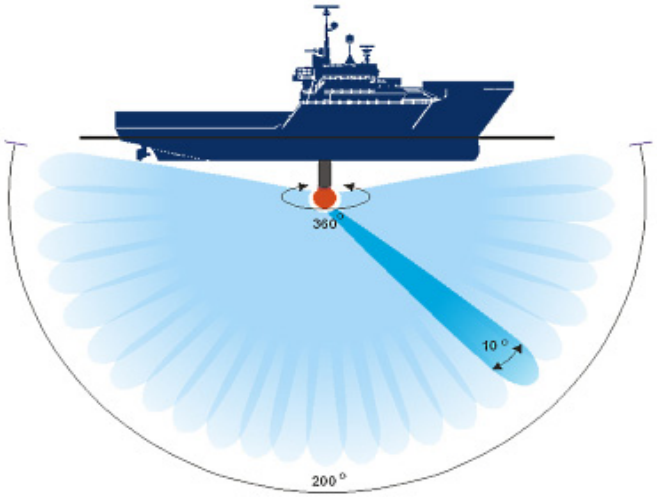

Fig. 3. Kongsberg Maritime HiPAP measurement principle

challenging due to the requirement of a pressure tolerant antenna. While a pressure tolerant molding satisfies part of this requirement it also leads to challenges related to damping and frequency shifts. Consequently a COTS antenna may not longer work as expected, and one might end up having to do a complete antenna re-design, where a single-frequency antenna is the easiest. This work has been done for the HUGIN AUVs where the GPS antenna (L1), WLAN, and Iridium are fitted in one molding, depth rated to 6000 m. The horizontal GPS accuracy for this unit is about 1.8 m (1σ).

It should be mentioned that the GPS receiver onboard the HUGIN AUVs may process DGPS and RTKGPS corrections. One possibility is to forward this information from e.g. the surface vessel to the AUV via a radio link or Iridium. Another alternative is to base the system on SBAS (satellite-based augmentation system). While neither are currently implemented it is believed that horizontal GPS accuracy somewhere between 0.6 and 0.2 m (1σ) is achievable for demanding AUV operations. Finally note that GPS PPP is not currently feasible for carrying out typical GPS surface fixes with an AUV since the technique requires fairly long sequences of data to converge.

2) Acoustic positioning: While acoustic time of flight navigation has been around for decades, it is still today the most reliable position aiding tool while (deeply) submerged. Several approaches are available [15], [16], where LBL and UBSL are the most common within AUV navigation. An increasing number of single-transponder and synchronous-clocks systems have also been proposed as alternatives to LBL and USBL. The reader is referred to [17], [18], [19], and references therein for a further treatment. Only USBL is discussed in this paper.

As for USBL, a typical approach is to measure the range and bearing (azimuth and elevation) of a transponder on the underwater vehicle relative to a transducer mounted on a surface vessel. A global position measurement, which may be transmitted to the submersible using an acoustic link, can be obtained by combining surface ship GPS and USBL measurements. The USBL principle is illustrated in Fig. 3 for the HiPAP USBL system. The following sources affect the combined GPS-USBL position estimate:

- GPS accuracy (as discussed in Section III-A.1)
- USBL measurement accuracy
- System installation accuracy
- Surface ship attitude accuracy
- Sound velocity profile (SVP) accuracy

A general expression for the north-east-down (NED) position of the AUV relative to the ship is given as

$$\boldsymbol{p}^n = \boldsymbol{R}_b^n(\phi,\theta,\psi)\boldsymbol{R}_t^b(\phi',\theta',\psi')\boldsymbol{p}^t(\Gamma,\alpha,\gamma), \tag{1}$$

where $\boldsymbol{p}^t \in \mathbb{R}^3$ is the position of the AUV measured relative to the USBL transducer, represented in the transducer reference frame $\{t\}$. The position vector $\boldsymbol{p}^t$ may be represented using spherical coordinates where Γ is the measured slant range, and α and γ are measured azimuth and elevation, respectively. Furthermore $\boldsymbol{R}_t^b \in SO(3)$ is a coordinate transformation matrix from $\{t\}$ to the ship reference frame $\{b\}$ (or alternatively, the rotation matrix from $\{b\}$ to $\{t\}$). The last matrix $\boldsymbol{R}_b^n \in SO(3)$ is the coordinate transformation matrix from $\{b\}$ to the NED frame $\{n\}$. The transformation matrices may be represented in many ways, but it is common to apply the *zyx*-convention using Euler angles [20]. The measured surface ship roll, pitch and heading are given by ϕ,θ,ψ, respectively, while ϕ',θ',ψ' describe the transducer alignment offset in roll, pitch and heading. Note that the latter angles are not geographical angles, but generic roll, pitch and heading Euler angles. Typically the transducer is mounted such that the latter angles are small. Note that the expression in (1) could have included an additional additive term $\boldsymbol{R}_b^n(\phi,\theta,\psi)\boldsymbol{p}_o^b$, where $\boldsymbol{p}_o^b$ is the offset (lever-arm) between $\{b\}$ and $\{t\}$. With the purpose of doing error analysis the term is however disregarded since linear offsets between $\{b\}$ and $\{t\}$ can be measured within millimeters (the same is also the case for the ship GPS antenna). The uncertainty introduced through $\boldsymbol{R}_b^n$ when doing lever-arm compensation is also negligible compared to the other error sources when $\|\boldsymbol{p}_o^b\| \ll \|\boldsymbol{p}^t\|$. For brevity it is assumed that $\{b\}$, $\{t\}$ and $\{n\}$ share the same origin.

A common approach in error analysis is to look at each isolated error source and to *propagate the uncertainties* [21]. This approach is used in this paper when analytical closed-form expressions are available. As for (1) a natural start is to look at the uncertainty in the horizontal position due to uncertainty in $\boldsymbol{p}^t$, i.e. USBL measurement uncertainty. If for the moment it is assumed that $\boldsymbol{R}_t^b$ and $\boldsymbol{R}_b^n$ are exact and equal to the identity matrix (all the angles are zero) we get that

$$\boldsymbol{p}^n = \boldsymbol{p}^t(\Gamma,\alpha,\gamma), \tag{2}$$

which means that an error in $\boldsymbol{p}^t$ directly translates to a (geographical) horizontal and vertical position error. With the assumption of small errors (first order approximation), the

TABLE I

AUV HORIZONTAL POSITION UNCERTAINTY (1σ) DUE TO HIPAP 500 MEASUREMENT UNCERTAINTY AT 20 DB AND 0.2 M (1σ) SURFACE SHIP GPS UNCERTAINTY. THE RELATIVE HORIZONTAL POSITION BETWEEN THE AUV AND THE USBL TRANSDUCER IS X = 50 M, Y = 50 M.

AUV depth [m]	50	100	500	1000	3000
AUV position uncertainty [m]	0.32	0.35	1.08	2.11	6.29

error in $\boldsymbol{p}^n$ may be approximated by

$$\boldsymbol{\Delta p}^n = \frac{\partial \boldsymbol{p}^t}{\partial \Gamma}\Delta\Gamma + \frac{\partial \boldsymbol{p}^t}{\partial \alpha}\Delta\alpha + \frac{\partial \boldsymbol{p}^t}{\partial \gamma}\Delta\gamma. \tag{3}$$

If $\boldsymbol{f} := \boldsymbol{p}^t$, $\boldsymbol{x} := [\Gamma, \alpha, \gamma]^\top$ and $\boldsymbol{\Delta x} := [\Delta\Gamma, \Delta\alpha, \Delta\gamma]^\top$, the same expression may be written in component form as

$$\Delta p_i^n = \sum_{j=1}^{3} \frac{\partial \boldsymbol{f}_i}{\partial \boldsymbol{x}_j}\boldsymbol{\Delta x}_j, \quad i = 1, \ldots, 3. \tag{4}$$

If the measurement error entries in $\boldsymbol{\Delta x}$ are independent, the position uncertainty along each axis may be stated in terms of the individual uncertainties, that is,

$$\sigma(\Delta p_i^n) = \sqrt{\sum_{j=1}^{3} \left(\frac{\partial \boldsymbol{f}_i}{\partial \boldsymbol{x}_j}\right)^2 \sigma(\boldsymbol{\Delta x}_j)^2}, \quad i = 1, \ldots, 3. \tag{5}$$

Disregarding the directional component (i.e. the covariance), the final horizontal position error may be approximated by the root-sum-square (RSS) of the horizontal components, that is,

$$\sigma(\Delta p_h^n) = \sqrt{\sigma(\Delta p_1^n)^2 + \sigma(\Delta p_2^n)^2}. \tag{6}$$

The USBL measurement accuracy depends on the signal-to-noise ratio (SNR). For HiPAP 500 the slant range uncertainty is typically < 20 cm while the angle uncertainties are $0.3°$, $0.18°$, and $0.12°$ at 0 dB, 10 dB and 20 dB, respectively (all 1σ). The uncertainty stated in (6) is calculated in Table I for a selection of depths. The contribution from surface ship GPS uncertainty is also included in the RSS calculation. In general the GPS uncertainty becomes negligible in deep waters.

A prerequisite for accurate USBL positioning is that alignment of the USBL transducer is well known. It is also eminent that the ship attitude accuracy is good. Any inaccuracies lead to a pointing error and hence a position error, as is evident from (1). If $\boldsymbol{p}^t$ and $\boldsymbol{R}_t^b$ are exact, and $\boldsymbol{R}_t^b$ equals the identity matrix, it follows that the horizontal position uncertainty due to uncertainty in the measured ship attitude can be calculated by applying (4)-(6), with $\boldsymbol{x} := [\phi, \theta, \psi]^\top$, $\boldsymbol{\Delta x} := [\Delta\phi, \Delta\theta, \Delta\psi]^\top$, and with $\boldsymbol{f} := \boldsymbol{R}_b^n(\phi, \theta, \psi)\boldsymbol{p}^t$. An attitude sensor used together with a UBSL system such as the HiPAP 500 should provide roll and pitch with an accuracy of about $0.01°$ (1σ) and heading better than $0.1°$ (1σ). The horizontal position uncertainty obtained by using these values are shown in Table II for a selection of depths.

The horizontal position uncertainty due to the USBL transducer alignment uncertainty (installation) can be derived analogously to the surface ship attitude. The expressions

TABLE II

AUV HORIZONTAL POSITION UNCERTAINTY (1σ) DUE TO SHIP ATTITUDE UNCERTAINTY OF $0.01°$ (1σ) IN ROLL AND PITCH, AND $0.1°$ (1σ) IN HEADING. THE SHIP ATTITUDE IS $\phi = 0°, \theta = 0°, \psi = 0°$. THE RELATIVE HORIZONTAL POSITION BETWEEN THE AUV AND THE USBL TRANSDUCER IS X = 50 M, Y = 50 M.

AUV depth [m]	50	100	500	1000	3000
AUV position uncertainty [m]	0.12	0.13	0.17	0.28	0.75

TABLE III

AUV HORIZONTAL POSITION UNCERTAINTY (1σ) DUE TO USBL TRANSDUCER ALIGNMENT UNCERTAINTY OF $0.05°$ (1σ) IN ROLL AND PITCH, AND $0.1°$ (1σ) IN HEADING. THE TRANSDUCER ALIGNMENT IS $\phi' = 0°, \theta' = 0°, \psi' = 0°$. THE RELATIVE HORIZONTAL POSITION BETWEEN THE AUV AND THE USBL TRANSDUCER IS X = 50 M, Y = 50 M.

AUV depth [m]	50	100	500	1000	3000
AUV position uncertainty [m]	0.14	0.18	0.63	1.24	3.71

in (4)-(6), are evaluated with $\boldsymbol{x} := [\phi', \theta', \psi']^\top$, $\boldsymbol{\Delta x} := [\Delta\phi', \Delta\theta', \Delta\psi']^\top$, and with $\boldsymbol{f} := \boldsymbol{R}_t^b(\phi', \theta', \psi')\boldsymbol{p}^t$. The uncertainty in the alignment angles is typically slightly higher than for the attitude sensor. For the HiPAP systems the transducer alignment values are obtained after interrogating a seabed transponder with a known absolute position. Roll and pitch accuracies better than $0.05°$ (1σ) and heading better than $0.1°$ (1σ) are expected. Horizontal position uncertainties obtained using these values are shown in Table III for different depths.

For a non-constant SVP the true acoustic sound path is in general not a straight line from the ship to the AUV. While the SVP only has a minor influence on the acoustic positioning near the transducer vertical (nadir), the sound profile must be measured and compensated for when the AUV operates far from the vertical (i.e. large elevation angles). The effect of errors in the SVP, and consequently the uncertainty associated with the ray-tracing, may be analyzed in different ways, see e.g. [12]. Another approach, which is utilized throughout this paper when discussing SVP uncertainty, is to do Monte Carlo (MC) simulations. In the simulations performed herein, additive noise is added to a presumed known SVP. When investigating the effect on the USBL positioning the ray-tracing is carried out repeatedly for a fixed arrival angle and propagation time. The fixed (deterministic) values are chosen such that ray-tracing with the known nominal SVP yields a desired vertical and horizontal end-point position.

The effect of SVP errors where investigated for the same relative AUV position and depths as in Table I-III. An example showing the variations in a real SVP over a ten day time period is shown in Fig. 4(a). The data were recorded outside Horten, Norway, in June 2010. In Fig. 4(b) the real SVP from June 14 was used as ground truth. The second SVP in the plot was obtained from the June 14 SVP and after adding stochastic noise. Other SVPs were also used as the considered ground truth. The uncertainty of the SVP was for all cases chosen to be 1 m/s (1σ) – evenly divided (in the

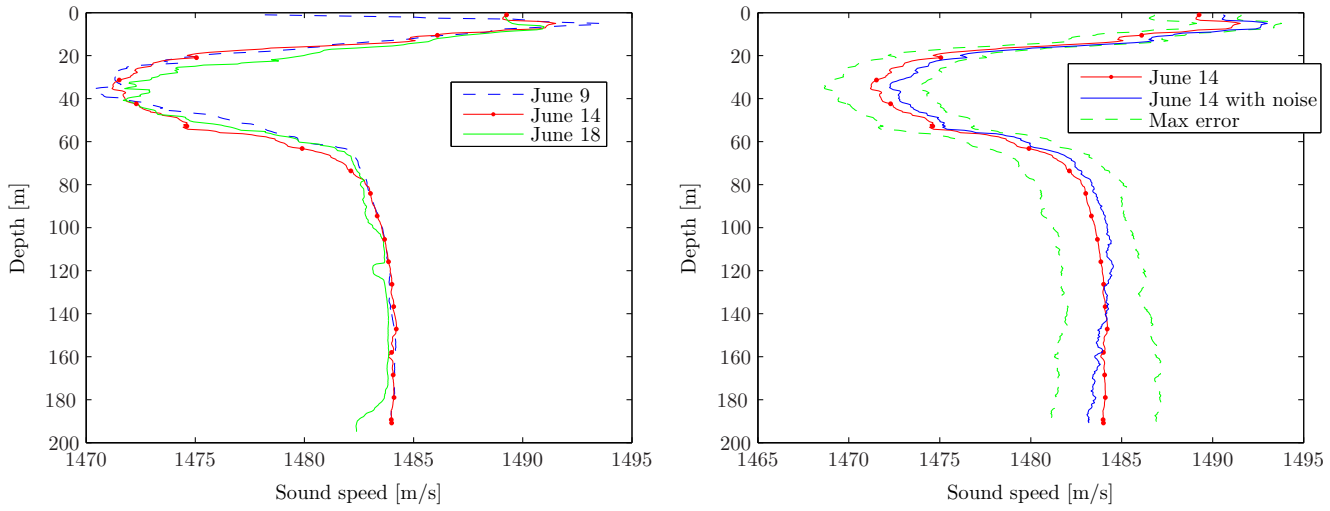

(a) (b)

Fig. 4. Sound velocity profile variability and simulation: (a) Real SVPs collected outside Horten, Norway, during a 10 day period in June 2010. (b) Simulated and ground truth SVP. The SVP uncertainty in the simulation was 1 m/s (1σ) – evenly divided (in the RSS sense) between a constant offset error model and a zero-mean first order Gauss-Markov error model. The green (dashed) lines are obtained by adding the minimum and maximum noises at each depth (resulting from 100 MC runs using the previously mentioned error models) to the true SVP.

RSS sense) between a constant offset error model and a zero-mean first order Gauss-Markov error model [22]. Other noise models could have been used, and in practise the SVP error often becomes smaller with depth due to stationary effects. The chosen models are therefore slightly conservative since the error distributions are considered equal at all depths. It was nonetheless found for all cases that the horizontal AUV position error due to SVP uncertainty is negligible compared to the other uncertainties in Table I-III. The impact on the total AUV positioning uncertainty is largest for large arrival angles. In the 50 m depth case the uncertainty was about 0.05 m (1σ).

It should be pointed out that commercially available sound velocity sensors have an accuracy in the sub-centimeter per second range. The uncertainty in the ray-tracing resulting from SVP errors is consequently only due to variations with time and space, where the latter typically is the most challenging. A rule of thumb is therefore to keep the horizontal offset between the AUV and the surface ship as low as possible throughout in order to minimize the sensitivity to SVP errors. Frequent SVPs should also be obtained if significant variations are expected. An overview of different SVP categories and further reading on ray-tracing (refraction) can be found in [23].

3) Aided inertial navigation system performance: As described in Section II-B an AUV may utilize a wide range of navigation sensors. It if furthermore well known that combining data from the different sensors will always be better than a single sensor alone. As mentioned, a modern AUV navigation system is typically based on INS and the use of a KF for carrying out the fusion of the disparate sensor data. The KF is only capable of estimating zero-mean time-varying errors with faster dynamics than the AINS error drift. The system is consequently well suited for removing errors attributed to e.g. white noise. Colored survey vessel attitude errors

TABLE IV

AUV AINS HORIZONTAL POSITION UNCERTAINTY (1σ) WITH GPS-HIPAP AIDING. THE NUMBERS ARE THE PREDICTED AINS UNCERTAINTIES, WITH THE SMOOTHED VALUES SHOWN IN BOLD TYPEFACE. THE RELATIVE HORIZONTAL POSITION BETWEEN THE AUV AND THE USBL TRANSDUCER IS X = 50 M, Y = 50 M.

AUV depth [m]	50	100	500	1000	3000
AUV position uncertainty [m]	0.30	0.31	0.68	1.07	2.20
	0.20	**0.21**	**0.43**	**0.69**	**1.45**

(assuming slower error dynamics than the AUV AINS error drift), SVP errors and survey vessel system installation errors are in general not observable while the AUV travels along a straight line. Some of these errors can become observable by maneuvering, but such effects are not discussed any further in this paper – straight line navigation is considered worst-case.

Compared to GPS-USBL alone, the results in the following illustrates the predicted improvement in the horizontal navigation accuracy when the AUV is fitted with a 0.8 nmi/h INS, a 600 kHz DVL, and a 0.01 % FS type pressure sensor. Such sensors are often found in modern AUVs today, including the HUGIN 1000 AUVs, as described in Section II-A. In addition to GPS-USBL, a second case is also considered where the only mean for position aiding is GPS fixes at the surface. In both the scenarios the AUV travels along a straight line at 2 m/s constant speed, and at constant heading and depth. GPS-USBL are available at 1/30 Hz throughout, while the AUV surfaces at various rates in the second case. The AUV receives GPS measurements for a duration of 2 min each time is surfaces.

All analyzes of the AINS performance were carried out using NavLab (Section II-B.1). As can be seen from Table IV the AINS clearly improves the overall position accuracy. The

TABLE V
AUV AINS HORIZONTAL POSITION UNCERTAINTY (1σ) WITH 1.8 M (1σ) SURFACE GPS FIXES AND FOR DIFFERENT SURFACING FREQUENCIES. THE NUMBERS ARE THE MAXIMUM PREDICTED AINS UNCERTAINTIES, WITH THE SMOOTHED VALUES SHOWN IN BOLD TYPEFACE.

	AUV position uncertainty [m]	
Fixes every 15 min	3.06	**1.22**
Fixes every 30 min	4.94	**2.02**
Fixes every 60 min	7.65	**3.25**

GPS-USBL uncertainties used in the simulation were based on Table I, and further assuming that 80 % of the HiPAP error is white and that 95 % of the GPS error is colored. As for the second case, Table V illustrates that it is possible to carry out (autonomous) high-precision AUV surveys with GPS surface fix as the only external positioning. As mentioned in Section II-B, a low drift velocity aided INS is required for all autonomous operations where external positioning is sparse. The HUGIN 1000 AUVs have proven in-situ DVL-aided INS performance on the order of 0.1 % of distance traveled (straight line). In the simulations the horizontal GPS accuracy was set to 1.8 m (1σ), which is the current GPS used on the vehicles. The effect of doing RTS smoothing is shown in Fig. 5. As described in Section II-B.1, the RTS smoother implemented in NavLab utilizes both past and future sensor measurements and KF covariances, hence significantly improving the accuracy.

B. Sounding Related Uncertainties

The following discuss uncertainties which are related to the bathymetric sensor and that contribute to the horizontal position uncertainty of the sounding footprint relative to the AUV. The HISAS sonar discussed in Section II-A is used as a case study. With a few exceptions, most of the material however also applies to MBE and traditional SSS as well.

1) Measurement uncertainty: As when discussing USBL, a natural starting point is to look at the fundamental measurement accuracy of the sensor. In light of (1) this relates to the uncertainty in the relative pointing vector, $\boldsymbol{p}^t$, from the sounding equipment to the sounding footprint. When discussing sounding related uncertainties, $\{b\}$ in the same expression now denotes the reference frame of the AUV navigation system. If for the moment it is assumed that $\boldsymbol{R}_t^b$ and $\boldsymbol{R}_b^n$ are exact, and $\boldsymbol{R}_b^n$ equals the identity matrix we get

$$\boldsymbol{p}^n = \boldsymbol{R}_t^b(\phi', \theta', \psi')\boldsymbol{p}^t(\Gamma, \alpha, \Phi), \tag{7}$$

where a depression angle Φ has been used instead of elevation. As can be seen from the expression an across-track sounding error in $\{b\}$ corresponds to an error in the (geographical) east direction, and similarly, along-track is in the north direction. Note that since a bathymetric sensor typically is a side-looking sensor, the nominal azimuth angle α in $\boldsymbol{p}^t$ is presumed zero.

As described in Section II-A, HISAS can collected bathymetric measurements in two different modes; HISAS sidescan and HISAS SAS bathymetry. For both modes there are in principle two factors which contribute to the measurement uncertainty. While not really the case, one can imagine that the HISAS sonar has (similar to a MBE) a sounding footprint for each pointing angle away from nadir. The first factor is then the position accuracy of the footprint itself, which is a function of the uncertainty in slant-range, Γ, and depression angle, Φ, relative to the interferometer. An illustration is given in Fig. 6. The second factor is related to the location of the sounding within the footprint. As will be discussed subsequently the size of the error is determined by the size of the footprint, or more precisely, the horizontal resolution of the sensor.

The resulting horizontal position uncertainty due to uncertainty in slant-range and depression angle can be found by evaluating (4)-(6) with $\boldsymbol{x} := [\Gamma, \Phi]^\top$, $\boldsymbol{\Delta x} := [\Delta\Gamma, \Delta\Phi]^\top$, and with $\boldsymbol{f} := \boldsymbol{R}_t^b\boldsymbol{p}^t(\Gamma, \alpha, \Phi)$. With the assumption that the SVP is known (see further discussed in Section III-B.4), the slant-range uncertainty is in the sub centimeter range (1σ) since the acoustic propagation time is determined with an accuracy in

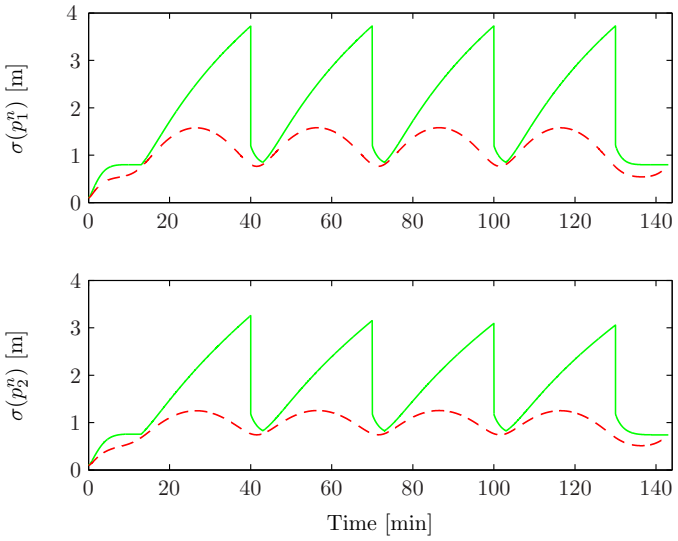

Fig. 5. Effectiveness of RTS smoothing. The estimated smoothed and real-time north and east position uncertainties (1σ) are shown in red (dashed) and green (solid), respectively. The data correspond to the 30 min case in Table V.

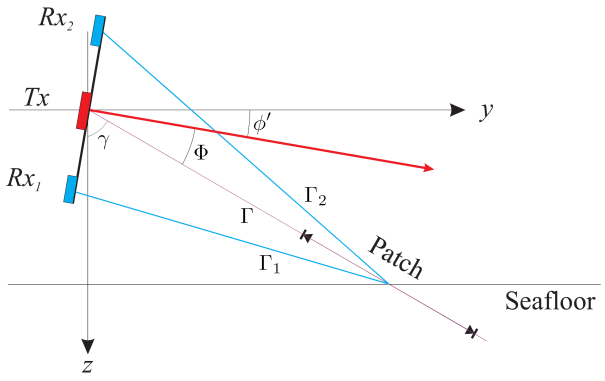

Fig. 6. Geometry for the HISAS interferometric SAS. The baseline distance I between Rx_1 and Rx_2 is 30 cm. When used on the HUGIN 1000 AUV, the sonar installation roll angle ϕ' is 22 ° about the AUV forward-aft axis.

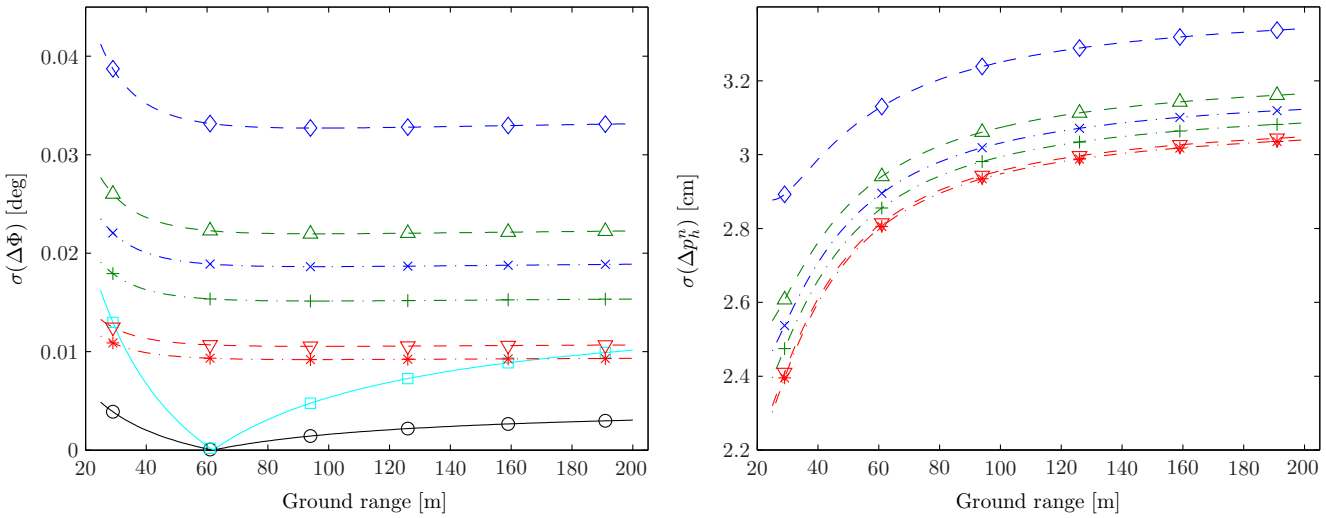

Fig. 7. Footprint position uncertainties for the HISAS sidescan and HISAS SAS bathymetry for 25 m AUV altitude: (a) Different contributions to the uncertainty in the depression angle. The contributions from baseline and sound speed uncertainties are shown as (□) and (○), respectively. The contributions from uncertainty in the time-delay estimate calculated from the CRLB are shown as (⋄), (×), and (∗) for 3 dB, 6 dB, and 12 dB, respectively. The same values calculated from the marginal probability density function are show as (△), (+), and (▽). (b) Horizontal position uncertainty due to uncertainty in the depression angle and slant-range. The different labels are the same as in (a) in terms of the time-delay estimator approach and SNRs.

TABLE VI
SOUNDING HORIZONTAL POSITION UNCERTAINTY (1σ) DUE TO SLANT-RANGE UNCERTAINTY OF 3 CM (1σ), TIME-DELAY UNCERTAINTY, SOUND SPEED UNCERTAINTY OF 0.3 M/S (1σ), AND BASELINE UNCERTAINTY OF 0.2 MM (1σ). THE AUV ATTITUDE IS $\phi = 0°, \theta = 0°, \psi = 0°$, AND THE SOUNDING SENSOR ALIGNMENT IS $\phi' = 22°, \theta' = 0°, \psi' = 0°$. THE HEIGHT OF THE AUV ABOVE THE ASSUMED FLAT SEABED IS Z = 25 M.

Ground range [m]	25	50	100	150	200
Beam elevation from nadir [°]	45.0	63.4	76.0	80.5	82.9
Depression angle [°]	23.0	4.6	-8.0	-12.5	-14.9
Position uncertainty [m] at 3 dB	0.03	0.03	0.03	0.03	0.03
Position uncertainty [m] at 6 dB	0.03	0.03	0.03	0.03	0.03
Position uncertainty [m] at 12 dB	0.02	0.03	0.03	0.03	0.03

the μs range. As for the uncertainty in the depression angle it is more complicated to determine since it depends on several factors, including SNR. As stated in [24] the depression angle can be calculated from

$$\Phi \approx \sin^{-1}\left(\frac{c\tau}{I}\right), \tag{8}$$

where c is the sound velocity at the sonar head, τ the difference in travel time, and I the baseline between the receiver banks. The uncertainty related to $\Delta\Phi$ can be found by evaluating (4)-(6) with $\boldsymbol{x} := [\tau, c, I]^\top$, $\boldsymbol{\Delta x} := [\Delta\tau, \Delta c, \Delta I]^\top$, and with $\boldsymbol{f} := \sin^{-1}(c\tau/I)$. As discussed in [11] it is possible to obtain a measurement for c in two ways; computation from CTD data or direct measurement. For a good quality CTD the first case yields an uncertainty for c on the order of 0.3 m/s (1σ), while commercially available sound velocity sensors have an accuracy in the sub-centimeter per second range (1σ). The CTD solution is currently used with the HISAS. As for the baseline I it can be determined to within 0.2 mm (1σ). The estimated time-delay τ is obtained from the sonar images, either from a complex-cross correlation as in HISAS sidescan mode, or from a maximum likelihood phase-difference estimator [25], [26], as in HISAS SAS bathymetry mode. Both methods also provide an estimate of the maximum normalized correlation coefficient (coherence), μ, which is related to the SNR as

$$\text{SNR} = \frac{\mu}{1-\mu}. \tag{9}$$

To assess the uncertainty in the time-delay estimate two different approaches are used. For the HISAS sidescan, a Cramer-Rao lower bound (CRLB) estimate obtained from the SNR and the number of independent pixels used in the cross-correlation estimate [27], [28], [29] is applied. For the HISAS SAS bathymetry the marginal probability density function of the interferometric phase-difference [30], [31] is integrated. According to [30] the CRLB is a better model in the presence of point scatterers while the marginal probability density function is best suited in the presence of speckle – the case for a general seafloor. The difference between the two estimates is most easily seen at low SNRs. This is also seen in Fig. 7(a) where the resulting uncertainty in the depression angle has been calculated for different SNRs and ground ranges. The uncertainties related to I and c have also been included in the plots. The predicted footprint horizontal position uncertainties due to the same uncertainties are shown in Fig. 7(b). As can be seen the from the graphs the introduced uncertainty is very small, independently of the time-delay uncertainty estimator. A summary is given in Table VI for the HISAS sidescan. The HISAS SAS bathymetry results only differed marginally.

As briefly mentioned above, and as will be discussed in the following, a significantly larger contribution to the horizontal footprint position uncertainty is related to the sensor resolution. The reason, which it is difficult the prevent completely, is that a particularly strong reflector or echo toward the edge of the resolution cell may pull the position estimate away from the true position at the footprint center. The problem is also well known for traditional MBE and SSS.

The horizontal resolution of the HISAS sidescan bathymetry is given by resolution along-track and by the length of the correlation window across-track. The resolutions are given as

$$dx_1 = 0.88\frac{\lambda}{D}\Gamma \tag{10}$$

$$dy_1 = L, \tag{11}$$

where λ is the signal wavelength, D is the along-track array length, and Γ is the slant-range. The HISAS has a signal wavelength of 15 mm (100 kHz) and an array length of 1.2 m. This corresponds to a 0.63° beam-width along-track. The across-track resolution is determined by the number of samples in the time-delay estimator. A larger number of samples will give a more accurate estimate at the expense of reduced along-track resolution. It has been chosen to use 128 samples, corresponding to a fixed across-track resolution of 3.2 m. For the HISAS sidescan this has been found to give an accurate and robust performance. The resolution is equivalent to an across-track beam-width of 1.47° at 50 m range, 0.37° at 100 m and 0.09° at 200 m (for a typical operating geometry). A sonar with the same vertical beam-width and an unambiguous beam (e.g. MBE in time of arrival-mode) would, at 100 kHz and 200 m range, have to be of size 9.5 m in the vertical plane.

The horizontal resolution is the primary difference between sidescan bathymetry and SAS bathymetry. Using a filter window of m along-track pixels and n across-track pixels, the HISAS SAS bathymetry resolutions are given by the theoretical SAS image resolutions times the filter sizes, i.e.

$$dx_2 = m\frac{d}{2} \tag{12}$$

$$dy_2 = n\frac{c}{2B}, \tag{13}$$

where d is the element size in the receiver array and B is the bandwidth. For HISAS, $d = 3.75$ cm and B is 30 kHz (typically). The preferred filter sizes are $m = n = 9$ pixels. The along-track resolution thus becomes 16.9 cm, and the across-track resolution 22.5 cm. The equivalent beam-widths are 0.19° by 0.10° at 50 m range, 0.10° by 0.03° at 100 m range and 0.05° by 0.01° at 200 m range.

With the assumption that the measured soundings are located within the footprint with some distribution or that a number of soundings are weighted accordingly, it is now possible to establish the horizontal position uncertainty from the horizontal resolution. Starting with the HISAS sidescan, it is common to assume that the along-track distribution is uniform [32], meaning that there is an equal chance of being anywhere within the footprint along that direction. It is easily found that the along-track position uncertainty at a certain beam elevation angle from nadir is given as a fixed percentage of the height. For the HISAS sidescan with 0.63° beam-width the along-track position uncertainty (1σ) in percentage of height is 0.4 % at 45.0°, 0.7 % at 63.4°, 1.3 % at 76.0°, 1.9 % at 80.5°, and 2.6 % at 82.9°. The beam angles are the the same as those investigated in Table VI. For the HISAS sidescan across-track position uncertainty the situation is slightly different, and several techniques are applied in the processing to enhance the resolution, and hence the accuracy. In the first step a mild Kaiser window is applied to suppress edge detections, approximately reducing the effective length L of the correlation window by a factor $3/4$ (see [33] for details). In the second step the cross-correlation estimate is biased towards zero with triangular weights, since an unbiased cross-correlator has an unacceptable large standard deviation. The uncertainty (1σ) associated with a triangular distribution is $a/\sqrt{6}$, where $a = 3/8\,L$ after running the Kaiser window. Note that the across-track uncertainty is fixed, and depends on the length of the correlation window (design parameter). It should be pointed out that even with weights it is not possible to prevent an infinitely strong reflector at the edge of the resolution cell to degrade the position accuracy. Experience with the HISAS sidescan has however shown that the techniques are effective.

For the HISAS SAS bathymetry no weights are applied. A conservative assumption is therefore to assume that the soundings are uniformly distritbuted within the resolution cell, and both in the along-track and across-track directions. The position uncertainties in along-track and across-track can then be found based on the resolutions stated in (12) and (13).

The resulting sounding horizontal position uncertainties due to sensor resolution are given in Table VII and Table VIII for a selection of geometries, and for the sidescan and SAS

TABLE VII

SOUNDING HORIZONTAL POSITION UNCERTAINTY (1σ) FOR HISAS SIDESCAN BATHYMETRY DUE TO SENSOR RESOLUTION. THE AUV ATTITUDE IS $\phi = 0°$, $\theta = 0°$, $\psi = 0°$, AND THE SOUNDING SENSOR ALIGNMENT IS $\phi' = 22°$, $\theta' = 0°$, $\psi' = 0°$. THE HEIGHT OF THE AUV ABOVE THE ASSUMED FLAT SEABED IS Z = 25 M.

Ground range [m]	25	50	100	150	200
Beam elevation from nadir [°]	45.0	63.4	76.0	80.5	82.9
Depression angle [°]	23.0	4.6	-8.0	-12.5	-14.9
Position uncertainty [m]	0.50	0.52	0.59	0.69	0.81

TABLE VIII

SOUNDING HORIZONTAL POSITION UNCERTAINTY (1σ) FOR HISAS SAS BATHYMETRY DUE TO SENSOR RESOLUTION. THE AUV ATTITUDE IS $\phi = 0°$, $\theta = 0°$, $\psi = 0°$, AND THE SOUNDING SENSOR ALIGNMENT IS $\phi' = 22°$, $\theta' = 0°$, $\psi' = 0°$. THE HEIGHT OF THE AUV ABOVE THE ASSUMED FLAT SEABED IS Z = 25 M.

Ground range [m]	25	50	100	150	200
Beam elevation from nadir [°]	45.0	63.4	76.0	80.5	82.9
Depression angle [°]	23.0	4.6	-8.0	-12.5	-14.9
Position uncertainty [m]	0.08	0.08	0.08	0.08	0.08

TABLE IX

SOUNDING HORIZONTAL POSITION UNCERTAINTY (1σ) DUE TO SOUNDING SENSOR ALIGNMENT UNCERTAINTY OF 0.5 MRAD (1σ) IN ROLL, AND 0.1° (1σ) IN PITCH AND HEADING. THE SOUNDING SENSOR ALIGNMENT IS $\phi' = 22^\circ, \theta' = 0^\circ, \psi' = 0^\circ$. THE HEIGHT OF THE AUV ABOVE THE ASSUMED FLAT SEABED IS Z = 25 M.

Ground range [m]	25	50	100	150	200
Beam elevation from nadir [°]	45.0	63.4	76.0	80.5	82.9
Depression angle [°]	23.0	4.6	-8.0	-12.5	-14.9
Sounding position uncertainty [m]	0.06	0.10	0.18	0.27	0.35

bathymetry. It is found that the across-track resolution is the dominating error source in the HISAS sidescan for low elevation angles. Compared to the fixed uncertainty in across-track of 0.49 m (1σ), the along-track uncertainty is 0.11 m (1σ) at 25 m ground range and 0.64 m (1σ) at 200 m. For the HISAS SAS bathymetry the uncertainty is more circular throughout.

2) Sensor alignment error: Similar to carrying out USBL positioning, a prerequisite for determining an accurate horizontal position of the sounding footprint is that the alignment of the sounding equipment is known with sufficient accuracy. Usually the AUV INS coordinate system is sought align with the standard vehicle body axes; forward, starboard, down. For brevity it is assumed in in this paper that they align exactly. Since the lever-arm between the INS and the payload typically is represented in the vehicle frame, any angle offsets between the body and the INS reference frames lead to a position error. For small offsets the introduced uncertainty is however negligible, and consequently disregarded in this work.

The uncertainty associated with the alignment between the AUV INS and the sounding equipment may be analyzed analogously to the alignment of the USBL transducer relative to ship reference frame. If $\{b\}$ in (1) now denotes the AUV INS coordinate system, $\boldsymbol{p}^t$ and $\boldsymbol{R}_b^n$ are exact, and $\boldsymbol{R}_b^n$ equals the identity matrix, the expressions in (4)-(6) can be evaluated with $\boldsymbol{x} := [\phi', \theta', \psi']^\top$, $\boldsymbol{\Delta x} := [\Delta\phi', \Delta\theta', \Delta\psi']^\top$, and with $\boldsymbol{f} := \boldsymbol{R}_t^b(\phi', \theta', \psi')\boldsymbol{p}^t$. Note that ϕ', θ', ψ' are not geographical angles, but generic roll, pitch and heading Euler angles.

For the HISAS SAS the alignment angles are estimated in two ways. The roll angle ϕ' is estimated by running two reciprocal lines with swath overlap. Due to the very wide swath and low grazing angles the roll angle can be found with an accuracy on the order of 0.5 mrad (1σ). As for the two remaining angles these are estimated in-situ by comparing the velocities from the INS with velocities (displacements) obtained in DPCA micro-navigation based on the SAS data. The angles are determined with an accuracy of about 0.1° (1σ). The predicted horizontal position uncertainties obtained by using these values are shown in Table IX for some geometries.

3) AUV attitude error: Similar to the alignment it is eminent that the AUV attitude accuracy is good. Any inaccuracy leads to a pointing error and hence a position error. If $\{b\}$ in (1) now denotes the AUV INS coordinate system, $\boldsymbol{p}^t$ and $\boldsymbol{R}_t^b$ are exact, and $\boldsymbol{R}_t^b$ equals the identity matrix, it follows that the horizontal position uncertainty due to uncertainty in the measured AUV attitude can be calculated by applying (4)-(6), with $\boldsymbol{x} := [\phi, \theta, \psi]^\top$, $\boldsymbol{\Delta x} := [\Delta\phi, \Delta\theta, \Delta\psi]^\top$, and with $\boldsymbol{f} := \boldsymbol{R}_b^n(\phi, \theta, \psi)\boldsymbol{p}^t$. The AUV attitude it is estimated by the AINS, either in-situ or in post-processing (see Section II-B.1). Typical uncertainties for the AINS found in the HUGIN 1000 AUVs are roll and pitch at about 0.004° (1σ) and heading at about 0.04° (1σ). The horizontal position uncertainty obtained by using these values are shown in Table X for a selection of geometries.

TABLE X

SOUNDING HORIZONTAL POSITION UNCERTAINTY (1σ) DUE TO AUV ATTITUDE UNCERTAINTY OF 0.004° (1σ) IN ROLL AND PITCH, AND 0.04° (1σ) IN HEADING. THE AUV ATTITUDE IS $\phi = 0^\circ, \theta = 0^\circ, \psi = 0^\circ$. THE HEIGHT OF THE AUV ABOVE THE ASSUMED FLAT SEABED IS Z = 25 M.

Ground range [m]	25	50	100	150	200
Beam elevation from nadir [°]	45.0	63.4	76.0	80.5	82.9
Depression angle [°]	23.0	4.6	-8.0	-12.5	-14.9
Sounding position uncertainty [m]	0.02	0.04	0.07	0.11	0.14

TABLE XI

DEEP WATER SOUNDING HORIZONTAL POSITION UNCERTAINTY (1σ) DUE TO SVP UNCERTAINTY OF 1 M/S (1σ). THE AUV ATTITUDE IS $\phi = 0^\circ, \theta = 0^\circ, \psi = 0^\circ$. THE HEIGHT OF THE AUV ABOVE THE ASSUMED FLAT SEABED IS Z = 25 M.

Ground range [m]	25	50	100	150	200
Beam elevation from nadir [°]	45.0	63.4	76.0	80.5	82.9
Depression angle [°]	23.0	4.6	-8.0	-12.5	-14.9
Sounding position uncertainty [m]	0.02	0.03	0.07	0.10	0.14

TABLE XII

SHALLOW WATER SOUNDING HORIZONTAL POSITION UNCERTAINTY (1σ) DUE TO SVP UNCERTAINTY OF 2 M/S (1σ). THE AUV ATTITUDE IS $\phi = 0^\circ, \theta = 0^\circ, \psi = 0^\circ$. THE HEIGHT OF THE AUV ABOVE THE ASSUMED FLAT SEABED IS Z = 25 M.

Ground range [m]	25	50	100	150	200
Beam elevation from nadir [°]	45.0	63.4	76.0	80.5	82.9
Depression angle [°]	23.0	4.6	-8.0	-12.5	-14.9
Sounding position uncertainty [m]	0.04	0.08	0.15	0.22	0.33

4) Sound velocity profile: The sounding footprint position uncertainty due to errors in the SVP may be analyzed similar to the USBL positioning by performing MC simulations. There are however two important differences. While the entire SVP above the AUV is of significance in the USBL case, only the SVP below the AUV is of importance for the horizontal sounding position. The second difference is the magnitude of the arrival angles, which for a side-looking sonar such as the HISAS SAS can be significant. Typical beam elevation angles relative to nadir are between 45 ° to 85 °, hence SVP errors are of greater importance than in typical USBL operations.

The fact that only the SVP below the AUV is of importance

for the HISAS means that the performance typically will vary more in shallow than in deep waters. As mentioned, the SVP error usually becomes smaller with depth, and consequently also the SVP error of importance to the sounding equipment. As discussed, commercially available sound speed sensors are available with an accuracy in the sub-centimeter per second range (1σ), making the associate sounding uncertainty negligible; independently of the beam elevation angle.

The effect of SVP errors are similar for the HISAS sidescan and HISAS SAS bathymetry. Two different cases are simulated, where one is for deep water, and one is for shallow water. The results are summarized in Table XI and Table XII. Only a constant error model is applied in the deep water case, while the first order Gauss-Markov model is applied in addition to the constant offset model in the shallow water case (the total SVP uncertainty is evenly divided between the two models).

Finally note that work has been done where the error in the SVP is estimated from overlapping MBE data [34], and consequently reducing the position (and depth) error. The technique may also be applied on HISAS sidescan and HISAS SAS bathymetry data.

C. Other Error Sources

While the list of error sources discussed above is fairly extensive, it is by no means complete. The need for accurate timing has not been discussed, but it is clearly a prerequisite – both for synchronization of payload and AUV navigation data, but also for synchronization of the AUV against the topside clock connected to the USBL positioning. In the HUGIN AUVs the payload sensors and the navigation system are synchronized against the same 1 PPS in-situ and will consequently not drift relative to each other. Before launch the AUV is also synchronized to GPS, and consequently also the HiPAP system. Several types of crystal oscillators may be used but most are 1 ppm or better. For a mission lasting for 24 h this corresponds to 86.4 ms. For an AUV traveling at 2 m/s forward speed this induces a 17 cm positioning error along-track. Oscillators with as low as 0.02 ppm drift are however available [18], making the problem negligible.

As for additional errors sources related to the sounding equipment one could mention contribution from 2pi wrapping and multipath. A further discussion is beyond the scope of this paper. The reader is referred to [35] for a further discussion.

IV. DTM Horizontal Error Budget

Based on the analyses and discussion on the different errors sources in Section III, it is possible to derive an error budget for the total horizontal mapping accuracy using AUVs. Under the assumption of statistically independent errors, the total DTM position uncertainty can be calculated by taking the RSS of the different error contributions. The resulting horizontal position uncertainties associated with the HISAS sidescan and HISAS SAS bathymetry alone are shown in Fig. 8. The uncertainty of the AUV AINS positioning using GPS-HiPAP is illustrated in Fig. 9. The uncertainties for a system with GPS-HiPAP and HISAS SAS bathymetry are shown Fig. 10

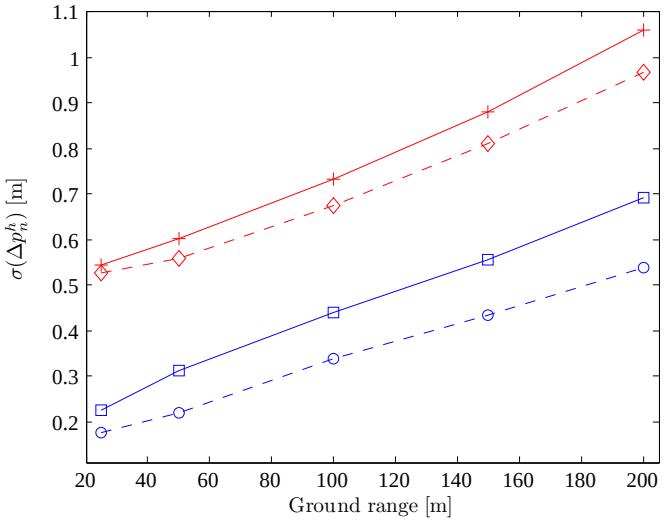

Fig. 8. Horizontal position uncertainty (1σ) due to horizontal position uncertainty in the HISAS sidescan and HISAS SAS bathymetry, alignment and AUV attitude uncertainty. HISAS sidescan with deep and shallow water SVPs is shown as ($\diamond$) and ($+$), respectively. HISAS SAS bathymetry with deep and shallow water SVPs is shown as ($\circ$) and ($\square$), respectively. The calculations are based on Table VI–XII and 25 m AUV altitude.

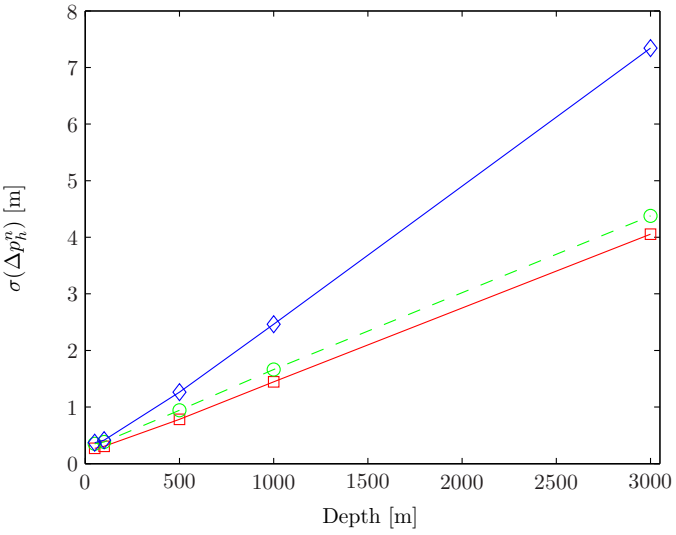

Fig. 9. Horizontal position uncertainty (1σ) for AUV AINS with GPS-HiPAP. The uncertainties are found from Table II–IV. Note that the values in Table I are not included since they are already embedded in Table IV. The real-time and smoothed uncertainties are shown as ($\circ$) and ($\square$), respectively. For comparison the uncertainties for the complete GPS-HiPAP system are shown as ($\diamond$). The latter values are calculated based on Table I-III.

for AUV depths 50 m and 500 m. The same figure also shows the application of AUV surface GPS, where the AUV surfaces every 15 min. Only the smoothed values are used for the AUV positioning uncertainties in the latter figure.

A. Hydrographic Survey Standards

As a response to the analyses and discussion above, a relevant question to ask is whether AUVs comply with the minimum standards suggested by the International Hydrographic Organization (IHO). A detailed description is given

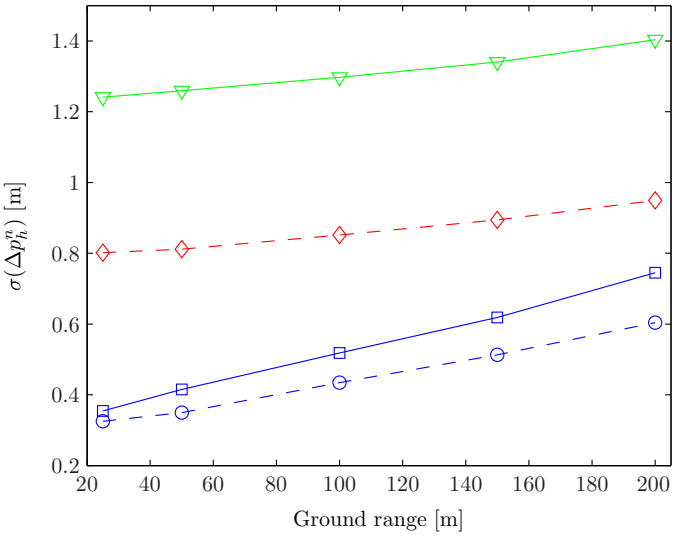

Fig. 10. Total horizontal mapping uncertainty (1σ). The uncertainty for a system based on 15 min interval surface fix from a GPS with 1.8 m (1σ) accuracy and HISAS SAS bathymetry in shallow water is shown as (▽). The remaining data are for the AUV AINS with GPS-HiPAP and HISAS SAS bathymetry. The data (◇) and (○) are for 500 m and 50 m AUV depth, respectively, and using deep water SVP. The data (□) is for 50 m AUV depth and with shallow water SVP. All the calculations are based on Table II–XII and 25 m AUV altitude.

in [36], where the different requirements are stated based on the survey type. The most strict requirements are found under the *special order* survey type, which embodies surveys in areas where under-keel clearance is critical, which for most cases is in areas never deeper than 40 m water depth. In terms of the required total horizontal accuracy of the DTM or nautical chart, it should be within 2 m (95 %). As stated in [36] the 95 % confidence level for the horizontal position is obtained by multiplying the 1σ standard deviations by a factor 2.45. Note that in the survey categories *1a* and *1b* (which are the next survey types after special order), the required horizontal position accuracy should be within 5 m + 5 % of depth (95 %). These are numbers which are fairly easily achieved with a state-of-the-art hydrographic AUV system, as shown in earlier sections. Complying with the special order requirement is on the other hand more challenging, though still possible.

As a first observation it is seen from Fig. 8 that the accuracy of the HISAS SAS bathymetry alone is within the 2 m (95 %) requirement for the entire swath. The HISAS sidescan bathymetry complies with the 2 m (95 %) requirement out to about 130 m and 150 m ground range in shallow and deep water, respectively. It is furthermore seen from Fig. 10 that the combination of HISAS SAS bathymetry and GPS-HiPAP at 75 m water depth also is within the 2 m requirement for the entire swath. The HiPAP system is of course also used in shallower water than 75 m (also at the surface); showing that an AUV like HUGIN 1000 with HiPAP and HISAS SAS bathymetry can be made to comply with the IHO special order.

As a second observation it is seen from Fig. 10 that hydrographic AUV systems based on surface fix GPS as the only external positioning still has some way to go, though it seems feasible. As mentioned in Section III-A.1 it may be possible to reduce the horizontal GPS uncertainty from 1.8 m (1σ) down to 0.6–0.2 m (1σ) by incorporating GPS corrections in-situ. To reduce the required surfacing frequency it is also necessary to improve the performance of the velocity-aided INS (when traveling in between position updates). A promising velocity aiding tool is DPCA (displaced phase centre antenna) micro-navigation. In DPCA the overlapping echoes from two independent pings are correlated in order to find the displacement of the SAS array, and consequently velocity information which can be used to aid the INS. If expectations are met, DPCA has an accuracy one order of magnitude better than DVL bottom-track [4]. A similar accuracy enhancement was also found in [37] when carrying out controlled experiments with a SAS mounted on a carriage on the seabed. A micro-navigated SAS system can be viewed as an extremely high quality correlation velocity log (CVL) [38]. Experiments with a HUGIN 1000 with HISAS are currently being planned in order to verify the in-situ accuracy of DPCA on AUVs, and the use of DPCA as an accurate INS aiding tool. It is believed by the author that a HUGIN 1000 with a high-accuracy vehicle GPS, HISAS DPCA velocity aiding, and HISAS SAS bathymetry can me made to comply with the IHO special order in terms of horizontal position accuracy. Such a system will also be able to carry out the surveys fully autonomous.

V. Conclusions

While traditional hydrographic surveys for creating e.g. nautical charts have been carried out using surface based systems, an increasing interest is shown toward the use of AUVs for the same purpose. An interesting and relevant problem, which unquestionably is of great importance to the end-user, is to determine the achievable accuracy in a DTM or nautical chart made from data collected by an AUV. This paper reports an in-depth discussion and analyses of the different components contributing to the horizontal DTM position accuracy. The HUGIN 1000 AUV fitted with HISAS 1030 interferometric SAS is used as a case study. It is concluded that excellent performance can be achieved and that state-of-the-art AUV systems with appropriate acoustic positioning can be made to comply with the IHO S-44 Special Order in terms of total horizontal position uncertainty. For AUV systems with GPS surface fix as the only external positioning there is still some way to go, though satisfying the requirements of the IHO S-44 Special Order seems feasible.

References

[1] N. Størkersen, H. Henriksen, and R. A. Klepaker, "Acoustically controlled untethered underwater vehicle systems for deep water seabed mapping," in *Proceedings from ISOPE 1996*, Los Angeles, CA, USA, 1996.

[2] R. E. Hansen, T. O. Sæbø, H. J. Callow, and E. H. P. E. Hagen, "Synthetic aperture sonar processing for the hugin auv," in *Proceedings of the IEEE Oceans Europe*, Brest, France, 2005.

[3] P. E. Hagen and R. E. Hansen, "Area coverage rate of synthetic aperture sonars," in *Proceedings of the IEEE Oceans Europe*, Aberdeen, UK, 2007.

[4] B. Jalving, K. Gade, O. Hagen, and K. Vestgård, "A toolbox of aiding techniques for the HUGIN AUV integrated inertial navigation system," in *Proceedings of the MTS/IEEE Oceans Conference and Exhibition*, San Diego, CA, 2003, pp. 1146–1153.

[5] P. E. Hagen, Ø. Hegrenæs, B. Jalving, Ø. Midtgaard, M. Wiig, and O. K. Hagen, "Making AUVs truly autonomous," in *Underwater Vehicles*. Vienna, Austria: In-Tech Education and Publishing, January 2009.

[6] Øyvind Hegrenæs, "Autonomous navigation for underwater vehicles," Ph.D. dissertation, Norwegian University of Science and Technology, 2010.

[7] K. Gade, "NavLab, a generic simulation and post-processing tool for navigation," *European Journal of Navigation*, vol. 2, no. 4, pp. 21–59, Nov. 2004, (see also http://www.navlab.net/).

[8] A. B. Willumsen and Ø. Hegrenæs, "The joys of smoothing," in *Proceedings of the IEEE Oceans Conference and Exhibition*, Bremen, Germany, 2009.

[9] B. Jalving, K. Vestgård, and N. Størkersen, "Detailed seabed surveys with AUVs," in *Technology and Applications of Autonomous Underwater Vehicles*, G. Griffiths, Ed. Taylor & Francis, 2003, vol. 2, pp. 179–201.

[10] R. M. Hare, "Depth and position error budgets for multi-beam echosounding," in *International Hydrographic Review*, Monaco, 1995.

[11] B. Jalving, "Depth accuracy in seabed mapping with underwater vehicles," in *Proceedings of the MTS/IEEE Oceans Conference and Exhibition*, Seattle, WA, USA, 1999, pp. 973–978.

[12] J. G. Blackinton, "Bathymetric resolution, precision and accuracy considerations for swath bathymetry mapping sonar systems," in *Proceedings of the IEEE Oceans Conference and Exhibition*, Honolulu, HI, USA, 1991.

[13] S. B. Bisnath and Y. Gao, "Innovation: Precise point positioning - a powerful technique with a promising future," *GPS World*, Apr. 2009.

[14] N. S. Kjørsvik and E. Brøste, "Using TerraPOS for efficient and accurate marine positioning," 2009.

[15] P. H. Milne, *Underwater Acoustic Positioning Systems*. Gulf Publishing Company, 1983.

[16] K. Vickery, "Acoustic positioning systems. A practical overview of current systems," in *Proceedings of the Autonomous Underwater Vehicles Workshop*, Cambridge, MA, USA, 1998, pp. 5–17.

[17] Ø. Hegrenæs, K. Gade, O. K. Hagen, and P. E. Hagen, "Underwater transponder positioning and navigation of autonomous underwater vehicles," in *Proceedings of the IEEE Oceans Conference and Exhibition*, Biloxi, USA, Oct. 2009.

[18] R. M. Eustice, L. L. Whitcomb, H. Singh, and M. Grund, "Experimental results in synchronous-clock one-way-travel-time acoustic navigation for autonomous underwater vehicles," in *Proceedings of the IEEE International Conference on Robotics and Automation (ICRA)*, Rome, Italy, Apr. 2007, pp. 4257–4264.

[19] S. E. Webster, R. M. Eustice, H. Singh, and L. L. Whitcomb, "Preliminary deep water results in single-beacon one-way-travel-time acoustic navigation for underwater vehicles," in *Proceedings of the IEEE/RSJ International Conference on Intelligent Robots and Systems*, St. Louis, MO, USA, Oct. 2009.

[20] T. I. Fossen, *Marine Control Systems: Guidance, Navigation and Control of Ships, Rigs and Underwater Vehicles*. Marine Cybernetics, 2002.

[21] J. R. Taylor, *An Introduction to Error Analysis: The Study of Uncertainties in Physical Measurements*. University Science Books, 1996.

[22] A. Gelb, *Applied Optimal Estimation*. The MIT Press, 1974.

[23] X. Lurton, *An Introduction to Undewater Acoustics: Principles and Applications*. Springer-Praxis, 2002.

[24] R. E. Hansen, T. O. Sæbø, K. Gade, and S. Chapman, "Signal processing for AUV based interferometric synthetic aperture sonar," in *Proceedings of the MTS/IEEE Oceans Conference and Exhibition*, San Diego, CA, USA, 2003, pp. 2438–44.

[25] D. C. Ghiglia and M. D. Pritt, *Two-Dimensional Phase Unwrapping: Theory, Algorithms, and Software*. New York, NY, USA: John Wiley & Sons, INC, 1998.

[26] T. O. Sæbø, B. Langli, H. J. Callow, E. O. Hammerstad, and R. E. Hansen, "Bathymetric capabilities of the HISAS interferometric synthetic aperture sonar," in *Proceedings of the MTS/IEEE Oceans Conference and Exhibition*, Vancouver, Canada, October 2007.

[27] A. H. Quazi, "An overview on the time delay estimate in active and passive systems for target localization," *IEEE Transactions on Acoustics, Speech and Signal Processing*, vol. ASSP-29, no. 3, pp. 527–533, 1981.

[28] A. Bellettini and M. A. Pinto, "Theoretical accuracy of synthetic aperture sonar micronavigation using a displaced phase-center antenna," *IEEE Journal of Oceanic Engineering*, vol. 27, no. 4, pp. 780–789, 2002.

[29] T. O. Sæbø, R. E. Hansen, and A. Hanssen, "Relative height estimation by cross-correlating ground-range synthetic aperture sonar images," *IEEE Journal of Oceanic Engineering*, vol. 32, no. 4, pp. 971–982, October 2007.

[30] R. F. Hanssen, *Radar Interferometry: Data Interpretation and Error Analysis*. Dordrecht, The Netherlands: Kluwer Academic Publishers, 2001.

[31] G. Franceschetti and R. Lanari, *Synthetic Aperture Radar Processing*. Boca Raton, FL, USA: CRC Press, 1999.

[32] E. Hammerstad, "Multibeam echo sounder accuracy," Kongsberg Simrad, Horten, Norway, EM Technical Note, 1998.

[33] H. L. Van Trees, *Optimum array processing. Part IV of detection, estimation, and modulation theory*. New York, USA: John Wiley & Sons Inc., 2002.

[34] M. Snellen, K. Siemes, and D. G. Simons, "An efficient method for reducing the sound speed induced errors in multibeam echosounder bathymetric measurements," in *Proceedings of Underwater Acoustics Measurements*, Nafplion, Greece, 2009.

[35] P. N. Denbigh, "Swath bathymetry: principles of operation and an analysis of errors," *IEEE Journal of Oceanic Engineering*, vol. 14, no. 4, pp. 289–98, Oct. 1989.

[36] International Hydrographic Organization. IHO standards for hydrographic surveys, 5th edition. Accessed on April 20, 2010. [Online]. Available: http://www.iho-ohi.net

[37] K. Gade, "Aiding inertial navigation with DPCA micronavigation," in *6th Mine Detection & Classification Joint Research Program Meeting*, NATO Undersea Research Centre, La Spezia, Italy, Nov. 2001.

[38] P. E. Hagen, R. E. Hansen, K. Gade, and E. Hammerstad, "Interferometric synthetic aperture sonar for AUV based mine hunting: The SENSOTEK project," in *Proceedings of Unmanned Systems*, Baltimore, MD, USA, 2001.